Chapter 5

The SAMPEX/PET data base and radiation belt model

At the Radiation Belt Workshop held at BIRA/IASB, 17–20 Oct 1995, J.B. Blake of Aerospace Corp. proposed that the observations of energetic proton fluxes made onboard of the SAMPEX satellite with the PET instrument be processed at BIRA/IASB by the TREND team with the aim of building a new trapped proton model. R.A. Mewaldt, PI for the SAMPEX/PET detector, supported this offer and during the spring of 1996, M.D. Looper from Aerospace Corp. visited BIRA/IASB to install the PET data on a DEC/Alpha station. The SAMPEX/PET data base installed at BIRA/IASB spans a time interval of four years during the declining phase of Solar Cycle 22.

This chapter contains a brief description of the SAMPEX mission and the PET instrument, and describes the data processing performed at BIRA/IASB and the new model that resulted.

5.1 The SAMPEX mission

The Solar, Anomalous, and Magnetospheric Particle EXplorer (SAMPEX) was the first SMall EXplorer (SMEX) mission. SAMPEX measures energetic electrons as well as ion composition of particle populations from ~ 0.4 MeV/nucleon to hundreds of MeV/nucleon from a zenith-oriented satellite in near-polar orbit. SAMPEX was successfully launched from NASA's Western Test Range (Lompoc, CA) at 1419 UT on 3 July 1992. The description of the SAMPEX satellite system and instruments has been taken from a series of papers in IEEE Trans. Geosci. Remote Sensing **31**, Nr. 3, 1993.

5.1.1 Spacecraft configuration

The SAMPEX spacecraft was designed to support a minimum mission duration of 1 year, with a mission goal of 3 or more years (Baker et al. 1993). The SAMPEX mechanical system basically consists of a primary structure, a deployable solar array system, and a yo-yo despin system.

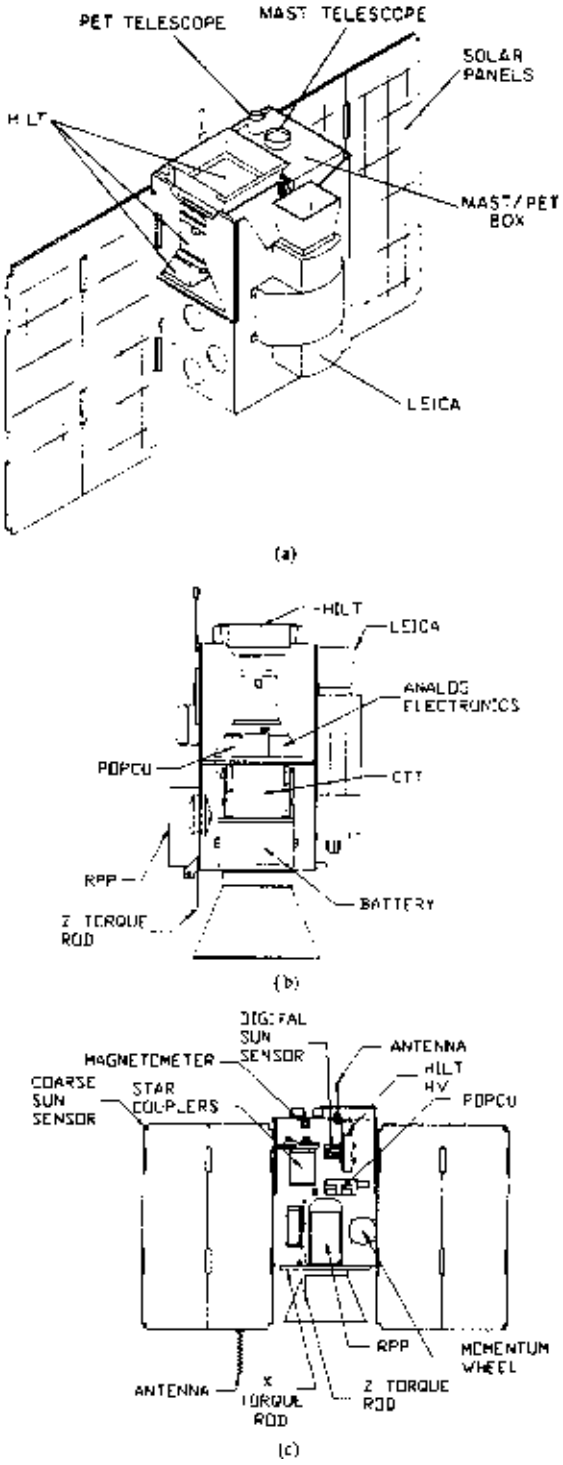

Figure 5.1. Mechanical design of the SAMPEX spacecraft and physical layout: (a) scientific instruments; (b) side view of subsystems; (c) back view of subsystem layout [from Baker et al. (1993)].

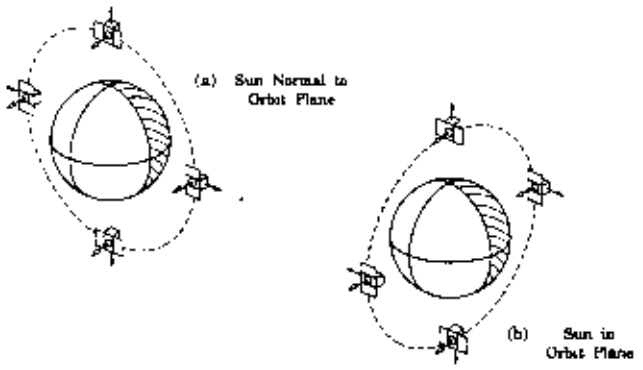

Figure 5.2. Pointing strategy for the SAMPEX spacecraft in two illustrative orbit planes [from Baker et al. (1993)].

SAMPEX is built up of machined aluminium plates which form a box-like structure that houses all of the spacecraft components (see Fig. 5.1).

The SAMPEX orbit has as inclination of $82°$, apogee of 670 km and perigee of 520 km. The orbit is non-Sunsynchronous and precesses through all local times (noon-midnight to midnight-noon) in about three months.

5.1.2 Attitude control

The Attitude Control Subsytem (ACS) is designed as a solar-pointed/momentum bias system. The SAMPEX spacecraft points at the Sun while it rotates about the sunline once per orbit in order to position the instrument lines-of-sight in the zenith direction when overflying the poles. Pointing requirements for the selected experiments are met by choosing sensor, torquers, and system configurations from a standard set of electronics, sensors and actuators. The ACS system utilizes one momentum wheel and three electromagnetic torque rods to orient the experiment viewing axis. Pointing ranges within $\pm 15°$ of vertical over the poles. The attitude computed onboard the spacecraft is known with an accuracy better than $2°$ (3σ). The pointing strategy for SAMPEX is to point the pitch axis (i.e. the normal to the solar panels) directly at the Sun. Then the yaw axis (parallel to the detector bore sights) rotates about the pitch axis once per spacecraft orbit. The spacecraft views north over the north pole, south over the south pole, and parallel to the equator during the equatorial plane crossings (see Fig. 5.2).

An Attitude Control Electronics (ACE) box which contains signal conditioning electronics and an independent analog safehold mode controls the ACS sensor and hardware. The onboard data system performs closed loop real-time attitude determination and control processing. Three-axis attitude determination is provided by comparing the local measured Sun vector and magnetic field vector with an on-board ephemeris model. Digital control of the spacecraft attitude is completed by sending appropriate command signals across the spacecraft data bus to the actuators.

Table 5.1. SAMPEX Scientific Instruments

	LEICA	HILT	MAST	PET
		Energy range (MeV)		
Electrons	—	—	—	0.4–30
H	0.76–6.1	—	—	18–250
He	0.45–6.1	4.3–38	7–20	18–350 MeV/nuc
C	0.44–11.4	7.2–160	14–210	34–120 MeV/nuc
Si	0.33–5.5	9.6–177	21–330	54–195 MeV/nuc
Fe	0.21–3.1	11.0–90	27–450	70–270 MeV/nuc
		Charge range		
Elements	1–25	2–28	2–28	1–2 (1–28*)
Isotopes	2–16	2	2–28	1–2 (1–10*)
		Physical characteristics		
Geometric factor ($\mathrm{cm}^2\mathrm{sr}$)	0.8	60	7–14	0.3–1.6
Field of view (deg, full angle)	24×20	68×68	101	58
Mass (kg)	7.4	22.8	8.8	(incl. with MAST)
Power (W)	4.9	5.6	5.3	(incl. with MAST)
Telemetry (kB/s)	1.3	0.9	1.4	0.5

*Commandable high-gain mode

The spacecraft determines the directions of the Sun and of the local magnetic field (using the Sun sensors and the magnetometer, respectively) with respect to the spacecraft's body-fixed coordinate frame, then compares these measurements with onboard calculations of the same quantitities in the GEI coordinate frame in order to relate the two frames. When the magnetic field is nearly parallel or antiparallel to the Sun line, the roll angle about their nearly common line is poorly determined. Therefore, when the angle between these two lines becomes less than 5° (or greater than 175°) while the spacecraft is out of eclipse, or less than 40° (or greater than 140°) while in eclipse, the spacecraft goes into "coast mode" and stops sending attitude information to the telemetry stream until the two lines diverge far enough to resume normal operations. Thus there is a gap in attitude information available on the ground. The time during which attitude is not being updated can add up to a large fraction of a day. The gaps in the attitude data were filled by interpolation, with a quality flag assigned to the interpolated data.

When the spacecraft enters coast mode, the magnetic torque rods shut off if they are running and the rotation speed about the Sun line is reset to a nominal value, which may be significantly slower than before coast mode began. On 27 May 1994, the spacecraft pointing strategy was changed to the effect that the instrument line of sight is perpendicular to the magnetic field while the spacecraft is in eclipse.

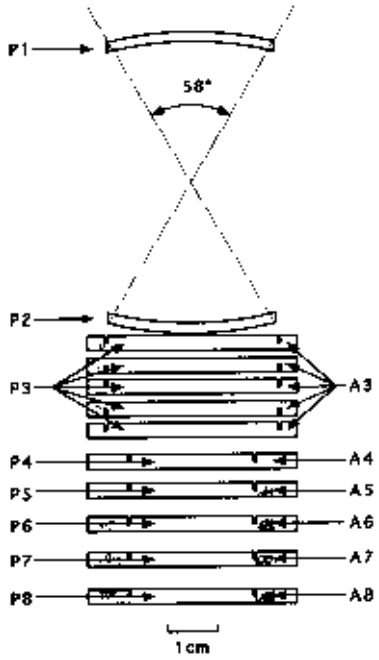

Figure 5.3. Schematic of the PET telescope. The primary analysis mode requires P1 and P2 (58° field of view). A wide angle 90° field of view that requires P2 and P4 but not P1 is also available for electrons. The regions labelled A4 through A8 are annular guard regions used to detect particles that enter or leave through the side of the stack [from Cook et al. (1993b)].

5.2 The Proton/Electron Telescope (PET)

The instruments on the SAMPEX spacecraft are the Low Energy Ion Composition Analyzer (LEICA), the Heavy Ion Large Telescope (HILT), the MAss Spectrometer Telescope (MAST), and the Proton/Electron Telescope (PET). The four instruments onboard have co-aligned boresights. A brief description of these instruments is given in Technical Note 5. The instrument characteristics are summarised in Table 5.1. In this study, only data from the PET are used.

The PET system is designed to complement MAST by measuring the energy spectra and relative composition of protons (18–250 MeV) and helium nuclei (18–350 MeV/nucleon) of solar, interplanetary, and galactic origins, and the energy spectra of solar flare and precipitating electrons from approximately 0.4 to 30 MeV. The instrument measures both trapped and precipitating energetic particles in different parts of the SAMPEX orbit. It also has the capability to look at manmade particle populations such as positrons which are emitted by nuclear reactors that have flown previously in low Earth orbit. The PET system can also duplicate and extend some measurement capabilities of MAST by providing energy spectra and elemental composition of nuclei from Li through Fe using a commandable high gain mode. It provides some isotopic information on nuclei from H to Ne.

Table 5.2. PET Detector, ADC, and discriminator characteristics

Detector Name	Nominal Thickness (mm)	Central Active Area (cm^2)	Guard Active Area (cm^2)	Nominal ADC Threshold (MeV)	Nominal ADC Full Scale (MeV)	Nominal Discriminator Thresholds (MeV)	Guard Discriminator Thresholds (MeV)
P1	2	8.0	—	0.35	157	P1A=3.1	—
P2	2	8.0	—	0.35	157	—	—
P3	15 (5×3) mm	9.2	4.5	0.7	317	P3A=2.8 P3B=12	0.3, 5
P4–P7	3	4.5	8.0	0.36	337	0.23	0.3, 1.2
P8	3	4.5	8.0	—	—	0.3	0.3, 1.2

5.2.1 Detailed description of the PET telescope

This section presents the description of PET by Cook et al. (1993b). The PET telescope, shown schematically in Fig. 5.3, consists of a series of eight Li-drifted silicon detectors (P1 to P8) with thicknesses ranging from 2 to 15 mm. The telescope opening aperture is defined by a passive collimator, followed by two curved (spherical) aperture detectors (P1 and P2) designed to minimise pathlength variations over the telescope's 58° opening angle. They are followed by six flat detectors (P3 to P8), where the P3 detector is comprised of five identical devices with a combined thickness of 15 mm. Detectors P3 through P8 are double-grooved devices with a central area for measuring energy loss and an annular guard region (labelled A in Fig. 5.3) used to detect particles that enter or leave through the side of the telescope, a design previously used on Voyager 1, Voyager 2 (Stone et al. 1977), and ISEE-3 (Althouse et al. 1978).

Particles satisfying the P1·P2 coincidence enter through a 1.5 cm long collimator (not shown in Fig. 5.3) that is nominally 0.75 mm thick at its thinnest point, and that preserves the 58° opening angle. The collimator also supports two windows (each 12.5 μm thick aluminised Kapton) that provide electrical shielding and protection from sunlight.

Detectors P1, P2, and the centre of P3 are each direct coupled to separate charge-sensitive pre-amplifiers, shaping amplifiers, and 10-bit ADCs. The summed output of the centres of P4 through P7 is fed into a fourth 10-bit ADC. The centre of P8 and the guard regions of P3 to P8 are each connected to pre-amplifiers, shaping amplifiers and discriminators. Each guard signal channel has two discriminators, A1 and A2: A1 is sensitive to minimum ionising particles while the A2 levels are ~ 1.2 MeV for A4–A8 and ~ 5 MeV for A3. Table 5.2 summarises the characteristics of the PET detectors and their analysis chains.

5.2.2 Analysis modes

PET Uses the conventional dE/dx-total energy technique to identify electrons, protons, and heavier nuclei, an approach which is based on the range-energy relations of energetic particles. With this approach a comparison of the rate of energy loss of energetic particles with their total energy loss can be used to identify both the charge and mass of energetic nuclei, as well as

Table 5.3. PET Response

Particle	Nominal Energy Interval (MeV or MeV/nuc)	Typical Geometry Factor[1] ($cm^2 sr$)	Detector[2,3] Combination	Associated counting rates Name	Res. (s)	Duty Cycle
Electrons	> 0.4	10	P1	P1	0.1	0.5
	$\sim$ 1–4	1.8	$\mathrm{P1} \cdot \overline{\mathrm{P1A}} \cdot \mathrm{P2} \cdot \overline{\mathrm{P3}} \cdot \overline{\mathrm{A}}$	ELO	6	1
	$\sim$ 4–20	1.7–1.1	$\mathrm{P1} \cdot \overline{\mathrm{P1A}} \cdot \mathrm{P2} \cdot \mathrm{P3} \cdot \overline{\mathrm{P4}} \cdot \overline{\mathrm{A}}$	EHI	6	1
	$\sim$ 12–30	0.5–0.3	$\mathrm{P1} \cdot \mathrm{P2} \cdot \mathrm{P4} \cdot \overline{\mathrm{P8}} \cdot \overline{\mathrm{A}}$	RNG	6	1
	$\sim$ 12–30	2.8–0.9	$\overline{\mathrm{P1}} \cdot \mathrm{P2} \cdot \overline{\mathrm{P3B}} \cdot \mathrm{P4} \cdot \overline{\mathrm{P8}} \cdot \overline{\mathrm{A}}$	EWG	6	1
H, He	> 4	10	P1	P1	0.1	0.5
	19–28	1.8	$\mathrm{P1A} \cdot \mathrm{P2} \cdot \overline{\mathrm{P3}} \cdot \overline{\mathrm{A}}$	PLO	6	1
	28–64	1.7–1.1	$\mathrm{P1A} \cdot \mathrm{P2} \cdot \mathrm{P3} \cdot \overline{\mathrm{P4}} \cdot \overline{\mathrm{A}}$	PHI	6	1
	64–85	0.5–0.3	$\mathrm{P1} \cdot \mathrm{P2} \cdot \mathrm{P4} \cdot \overline{\mathrm{P8}} \cdot \overline{\mathrm{A}}$	RNG	6	1
	> 85	0.3	$\mathrm{P1} \cdot \mathrm{P2} \cdot \mathrm{P8} \cdot \overline{\mathrm{A}}$	PEN	6	1
$Z \geq 3$ Nuclei[4]	60-200	1.7–1.1	$\mathrm{P1} \cdot \mathrm{P2} \cdot \overline{\mathrm{P4}} \cdot \overline{\mathrm{A}}$	PLO, PHI	6	1

[1] Based on calculation with straight tracks; accelerator calibration data will modify values for electrons.
[2] "A" Represents the logical "OR" of the guard rings on P3 to P8.
[3] P1A, P3A, and P3B are digital discriminators on the P1 and P3 outputs set at 3.1, 2.8, and 12 MeV, respectively.
[4] Commandable mode for $Z \geq 3$ nuclei; energy range indicated is for Si-28.

measure their kinetic energy. In practice, the rate of energy loss is determined by measuring the energy loss (ΔE) in a detector of known thickness, such as P1 or P2 on PET. In order to minimise the variations in the path length over the telescope's 58° opening angle, P1 and P2 have been constructed from spherical segments of silicon. As a result, PET should be capable of identifying elements from H to Ni, with isotope identification extending through Ne. Although the range-energy characteristics of electrons are not nearly so precise as those of nuclei, electrons are easily separable from protons because of their much lower rate of energy loss.

PET Includes a number of separate analysis modes that are designed to identify electrons and nuclei over selected energy intervals: the primary Lo-Z mode providing differential energy spectra of electrons and of H and He nuclei, and the commandable Hi-Z mode (in which the gain of P1, P2, and P3 is reduced by a factor of ten) in which energy spectra of the elements from Li to Ni can be measured as well. The data used in this study were obtained in the Lo-Z mode only.

The pulse height of an event is triggered whenever one of the coincidence equations in Table 5.3 is satisfied. The results, along with other information such as the state of various discriminators, are stored in one of five separate event buffers. These event buffers are read out into the telemetry stream by a rotating priority system that ensures that all event types are represented under conditions that range from periods dominated by intense fluxes of solar flare nuclei to periods dominated by trapped protons and electrons.

Because the telemetry rate is insufficient to transmit every event, rate accumulators are used to count events during 6 s intervals. A total of 32 such "counting rates" record instrument live-time, the frequency of electrons and nuclei in several energy intervals defined by the coincidence

Table 5.4. SAMPEX/PET Data set file description

File names	File contents
EPHxxxxx.DAT	Ephemeris data
PTLVxxxxx.DAT	Livetimes
PKTSxxxxx.DAT	Count rates

logic, and the triggering frequency of a variety of discriminator levels. Table 5.3 summarizes some of the counting rates of physical interest. In addition, the "singles" counting rate of the front detector (P1) is sampled for 0.05 s out of every 0.10 s to measure the flux of magnetospheric electrons > 0.4 MeV and protons > 4 MeV on a fast time scale. This "high resolution" rate is recorded whenever the count rate exceeds a (commandable) level of ~ 50 counts/s. All of the coincidence equations and some of the discriminator levels can be modified by command to allow for the possibility of noisy or failed detectors, and to optimise the instrument's response to the various particles of interest.

5.2.3 Calibrations

The response of PET to electrons has been calibrated over the energy range from ~ 0.3 MeV to ~ 27 MeV with electron beams incident at a variety of energies and zenith angles. At higher energies the linear electron accelerator at the EG&G Santa Barbara facility was operated in a low intensity mode to provide mono-energetic beams at fourteen separate energies from 1.5 to 27 MeV. Calibrations at somewhat lower energies (0.3 to 3 MeV) were carried out with a β spectrometer. PET Was also calibrated with radioactive sources to determine its positron detection efficiency and its response to γ rays that Compton scatter in the telescope producing a possible background for electron and positron measurements. For accelerator calibrations, where beam time is often limited and expensive, PET has a special port that allows events to be read out at rates of several thousand per second.

PET Has a built-in calibrator that can be initiated either periodically (every 6.8 hours) or by command (Cook et al. 1993a). The calibrator includes an 8-bit DAC that supplies reference voltages to the test pulsers of each of the signal channels. The test pulsers can be stimulated either individually or in groups to perform limited tests of the coincidence logic, measure the thresholds of the various discriminators, and the gain, linearity, and long-term stability of the ADCs. Calibration "events" are flagged and stored in a special buffer for read-out and telemetry along with the regular data.

5.3 The SAMPEX/PET data base

The SAMPEX/PET data base was delivered to BIRA/IASB by M.D. Looper on optical disks. The data set consists of ephemeris files, attitude information, count rates and livetimes. The data delivered to BIRA/IASB cover the period from the start of the mission (day 187 of 1992) up to day 121 of 1996.

The PET data base was installed on a DEC Alpha workstation running OpenVMS. The data analysis was performed with a series of IDL programs and the `UNILIB` library. The analysis is described in detail in Technical Note 5. The data base is stored as a series of files, each containing data for one day, with the date forming the second part of the file name as `YYDDD`. Table 5.4 list the different file types that make up the data base.

The contents of each file in Table 5.4 correspond to an IDL structure. The structures are defined as:

```
nkts = 14400
eph = replicate({time:0l,alt:0.,lon:0.,lat:0.,pa:0.,b:0.,
                 fl:0.,bc:0.,flc:0.,beta:0.,bv:fltarr(3),
                 vn:fltarr(3),altm:0.,flag:0b},nkts)
ptlv = replicate({plo:0.,phi:0.,rng:0.,pen:0.},nkts)
pkts = replicate({p21:0b,p22:0b,p23:0b,p24:0b,p31:0b,p32:0b,
                  p33:0b,p34:0b,p4:0b,p5:0b,p67:0b,p81:0b,
                  p82:0b,p83:0b,p84:0b,d31:0b,d32:0b,d33:0b,
                  d34:0b,d4:0b,d5:0b,d67:0b},nkts)
```

`nkts` Is the number of six second intervals per day.

5.3.1 PTLVxxxxx.DAT

The `PTLV` structure contains the livetimes in seconds (maximum 6 s) over each six second interval:

ptlv.plo livetime (s) for 2-detector (PLO) events;

ptlv.phi livetime (s) for 3-detector (PHI) events;

ptlv.rng livetime (s) for 4-detector (RNG) events;

ptlv.pen livetime (s) for 8-detector (PEN) events.

5.3.2 PKTSxxxxx.DAT

The `PKTS` structure contains the counts of protons and deuterons over each six second interval:

pkts.p* counts of proton events from start to end of interval;

Table 5.5. PET Channel characteristics

Channel (PKTS)	Buffer (PTLV)	Energy Range (MeV/nuc)	Nominal Geometric Factor (cm^2sr)
p21	plo	18.5–20.5	1.792
p22	plo	20.5–22.5	1.792
p23	plo	22.5–24.5	1.792
p24	plo	24.5–27.2	1.792
p31	phi	27.2–37.4	1.714
p32	phi	37.4–45.8	1.527
p33	phi	45.8–53.0	1.356
p34	phi	53.0–65.4	1.146
p4	rng	65.4–71.0	0.477
p5	rng	71.0–76.3	0.420
p67	rng	76.3–86.1	0.341
p81	pen	86.1–120.0	0.277
p82	pen	120.0–200.0	0.277
p83	pen	200.0–300.0	0.277
p84	pen	300.0–500.0	0.277
d31	phi	18.4–25.4	1.714
d32	phi	25.4–31.0	1.527
d33	phi	31.0–36.0	1.356
d34	phi	36.0–44.3	1.146
d4	rng	44.3–48.1	0.477
d5	rng	48.1–51.7	0.420
d67	rng	51.7–58.2	0.341

pkts.d* counts of deuteron events from start to end of interval.

Table 5.5 associates the count rates in PKTS with the livetimes in PTLV, and gives energy ranges and nominal geometry factors for each channel. When a livetime is zero in the PTLV structure, all associated count rates should be discarded.

5.3.3 SCEWxxxxx.DAT

For the anisotropy study described in TN 6 Part II, the values of L and B calculated at the guiding centre corresponding to each measurement are needed. The SCEW structure contains $\Delta L \equiv L_{\rm GC} - L$ and $\Delta B \equiv B_{\rm GC} - B$ at the start of each six second interval: The SCEW data are not used in this study. Instead, we chose to regenerate the values of B, L with the DGRF or IGRF model for the epoch of Jan 1 of each year of measurements. Using the quaternions in the

Table 5.6. Description of the EPH structure

Element	Data Type	Definition
eph.time	Long integer	Universal time (s) of start of six second interval
eph.alt	Single precision	Geodetic altitude (km)
eph.lon	Single precision	Longitude (deg)
eph.lat	Single precision	Geodetic latitude (deg)
eph.pa	Single precision	Pitch angle (deg)
eph.b	Single precision	DGRF Magnetic field intensity (Gauss) at spacecraft location
eph.fl	Single precision	L Value (R_{E}) corresponding to spacecraft location and eph.pa
eph.bc	Single precision	DGRF Magnetic field intensity (Gauss) at the guiding centre of a 100 MeV particle
eph.flc	Single precision	L Value (R_{E}) corresponding to the guiding centre of a 100 MeV particle and eph.pa
eph.beta	Single precision	Azimuthal angle β (deg)
eph.bv	Single precision (3)	Geocentric spherical DGRF magnetic field vector components (Gauss)
eph.vn	Single precision (3)	Geocentric spherical components of the local curvature vector of the magnetic field
eph.altm	Single precision	Altitude of the lowest mirror point on the local magnetic field line
eph.flag	Byte	Quality flag

QCORxxxxx.DAT, the look direction of the instrument and the locations of the guiding centres corresponding to each measurement and particle energy E were determined, and the values of B_{GC} and the respective $L_{\mathrm{GC}}(E)$ were calculated. Finally, a new value of the pitch angle for each measurement was derived from the look direction and the direction of the local magnetic field vector. The resulting values are stored in the new ephemeris files described in Sect. 5.3.4.

5.3.4 Generation of a new ephemeris data set

In order to simplify the data processing, a new set of ephemeris files was generated: the EPHxxxxx.DAT files. Each of these files combines all the ephemeris, attitude and magnetic field data for one day. The magnetic field vectors and related quantities were recalculated from the ephemeris data using the UNILIB library and DGRF 90 or IGRF 95 updated to Jan 1 of the year of the measurements (see Sect. 5.3.3).

Table 5.6 lists the definitions of the structure elements. eph.beta Is the azimuthal angle β defined in TN 6 Part II. The values of L_{GC} and B_{GC} correspond to the guiding centre positions

of 103.05 MeV protons (centre of energy channel `p81`). Storing one value of $L_{\rm GC}$ and $B_{\rm GC}$ is sufficient as they depend linearly on the gyroradius.

5.4 Model construction

In this section the data binning procedure is outlined, as well as the conversion from counts and livetimes to fluxes. The model construction procedure is analogous to the procedure followed for the AZUR data (see Sect. 4.3). The correction procedure for the field of view, described in general terms in Appendix A, is adapted to the PET telescope and sensors.

5.4.1 Data binning

The PET data for the second half of 1994 and the first half of 1995 have been averaged over a rectangular three dimensional bin in (E, L, α_0) space by means of the IDL programme `BINNING.PRO`. The (E, L, α_0) bin limits of the grid are listed in Table 5.7. The limits of the energy bins correspond to the channel limits in Table 5.5. The L and α_0 bins were selected so as to obtain a uniform distribution of the measurements over the grid. The DGRF magnetic field model for epoch 1995 was used to calculate the magnetic coordinates. No external magnetic field model was used.

Because of the relatively poor statistics of the PET proton counts (only a fraction of the events satisfying detector coincidence conditions are actually processed by the pulse height analysers, and only a few of the twenty analysed events telemetred per second appear in the proton channels; see Technical Note 5), it is not possible to convert individual count rates into fluxes without accumulation. For many measurements, the recorded count rate is zero while the corresponding livetime is not, and is lower than the integration time of 6 s. Therefore, it was decided to average the counts and livetimes separately, so that the average flux in each model bin is the ratio of the sum of the counts in that bin divided by the sum of the livetimes.

5.4.2 Correction for telescope field of view

As for the AZUR data, the PET flux averages are corrected for the telescope field of view by means of the program `FOVAPP.PRO`. Figure 5.4 shows the effective areas for a subset of the PET sensors, which were provided in the form of a table by M.D. Looper.

There are eleven ranges in Fig. 5.4, corresponding to particles stopping in each of the detector wafers from P2 to P8 (counting the P3A, ..., P3E wafers separately) after passing through all the previous detectors starting with P1. With reference to the channels listed in Table 5.5, p21–p24 are P2 range, p31 is P3A, p32 is P3B, p33 is P3C, p34 is the sum of particles with ranges to P3D and P3E (so its response is taken to be the average of the responses for P3D and P3E), p4 is P4, p5 is P5, p67 is P6 and P7 totalled (and again responses averaged), and p81–p84 are all of P8 range.

Table 5.7. (E, L, α_0) Bin limits for the PET model grid

E Limits (MeV)	L Limits (R_{E})	α_0 Limits (deg)
18.5	1.005	0.0000
20.5	1.015	21.2018
22.5	1.025	22.7340
24.5	1.035	24.2568
27.2	1.045	25.7705
37.4	1.055	27.2751
45.8	1.065	28.7709
53.0	1.075	30.2579
65.4	1.085	31.7364
71.0	1.095	33.2065
76.3	1.105	34.6683
86.1	1.115	36.1220
120.0	1.125	37.5677
200.0	1.135	39.0055
300.0	1.145	40.4356
500.0	1.155	41.8581
	1.165	43.2730
	1.175	44.6806
	1.185	46.0809
	1.195	47.4741
	1.205	48.8602
	1.225	50.2394
	1.275	51.6118
	1.325	52.9774
	1.375	54.3364
	1.425	55.6888
	1.475	57.0348
	1.525	58.3744
	1.575	59.7078
	1.625	61.0350
	1.675	62.3561
	1.725	63.6712
	1.775	64.9803
	1.825	66.2836
	1.875	67.5812
	1.925	68.8730
	1.975	70.1592
	2.025	71.4399
		72.7150
		73.9848
		75.2492
		76.5084
		77.7624
		79.0112
		80.2549
		81.4936
		82.7273
		83.9562
		85.1802
		86.3994
		90.0000

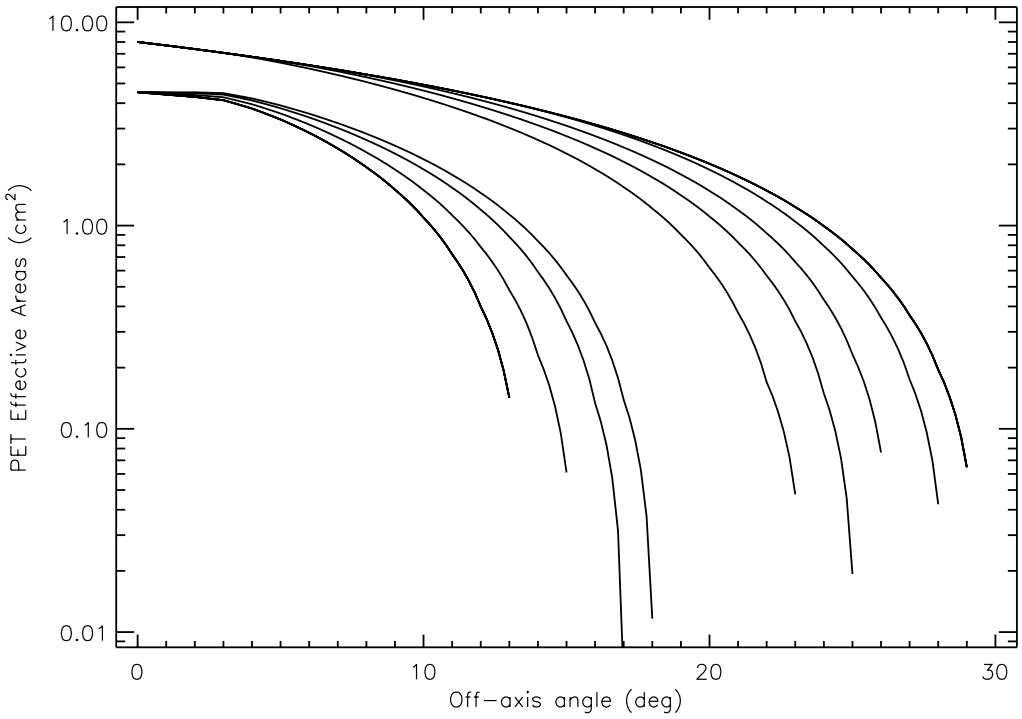

Figure 5.4. Effective areas of the SAMPEX/PET sensors

The IDL program `AREAS.PRO` reads the tabulated effective areas and returns the areas for all fifteen proton channels. The field of view correction is carried out by the program `DETCOR.PRO`, which calls `FOVAPP.PRO` and `AREAS.PRO`.

5.4.3 Final flux map

The IDL program `MODEL.PRO` reads in the flux averages created by `BINNING.PRO` and writes the final flux map `SAMPEX.DAT`. This program is interactive and allows for the correction of spurious points. For grid points where there are no data, the flux is set to -1.0.

The final flux map is then transformed into a `BLOCK DATA` file by means of the program `MODTOBD.FOR`. This program also transforms differential into integral fluxes. The implementation of the new SAMPEX model (called PSB97) in `UNIRAD` is described in Technical Note 10.

5.4.4 Comparison to AP-8

Figures 5.5–5.8 show the flux maps of the PSB97 model for channels 1, 5, 9, and 13, respectively, in (L, α_0) space, together with the directional AP-8 MIN maps for the same grid values.

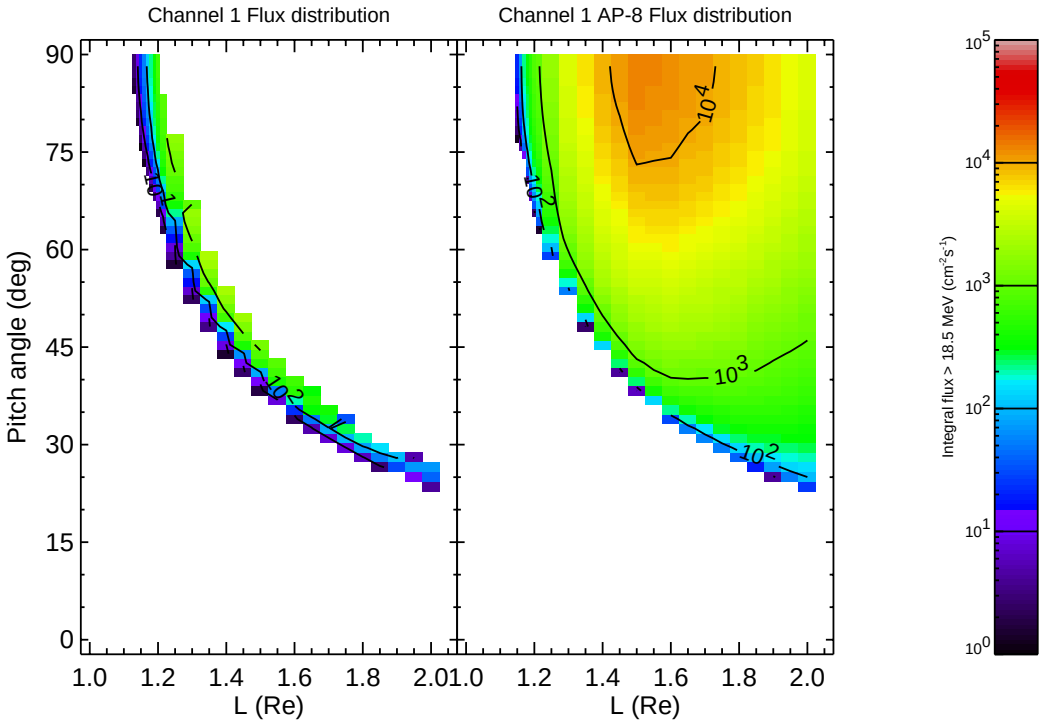

Figure 5.5. (L, α_0) Map of the PSB97 model and AP-8 MIN for channel 1

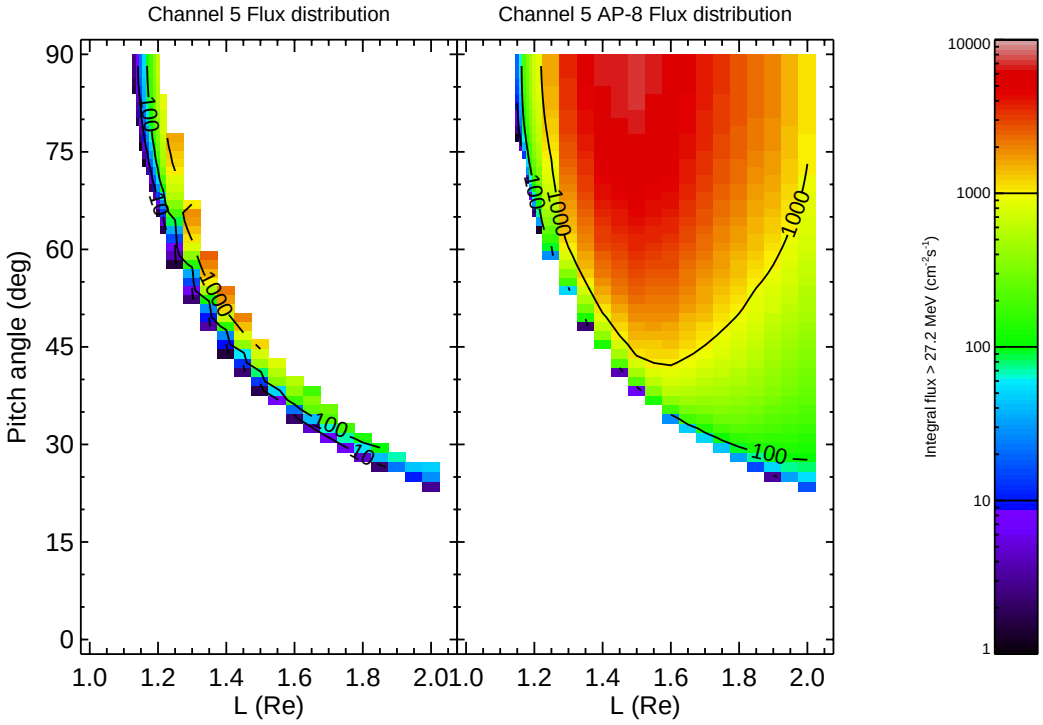

Figure 5.6. (L, α_0) Map of the PSB97 model and AP-8 MIN for channel 5

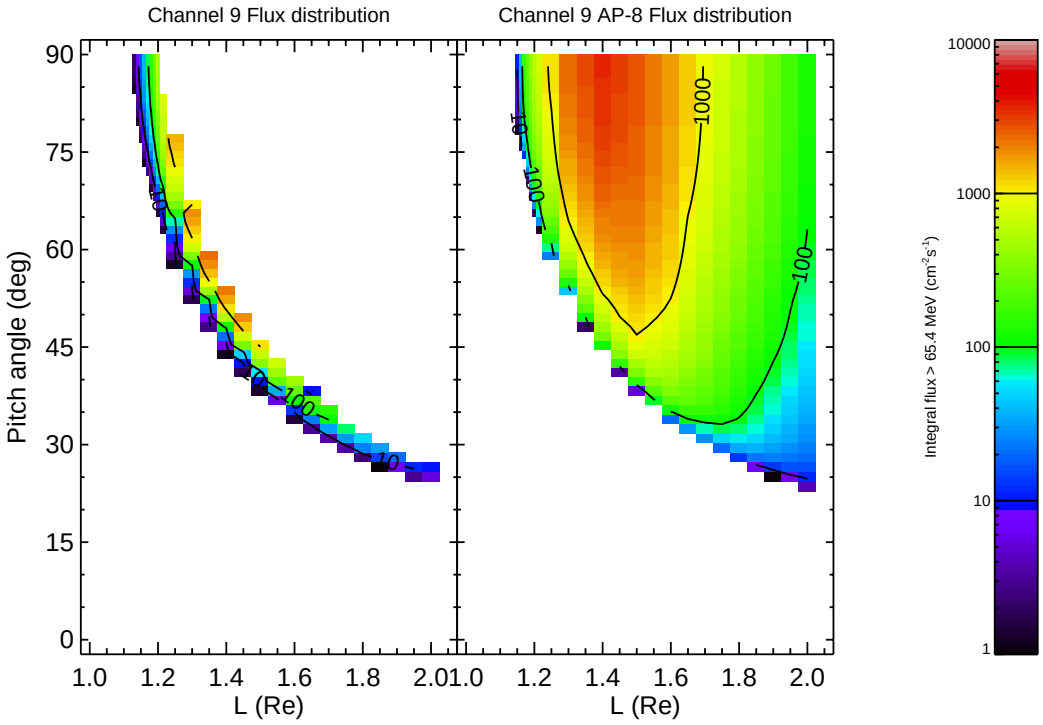

Figure 5.7. (L, α_0) Map of the PSB97 model and AP-8 MIN for channel 9

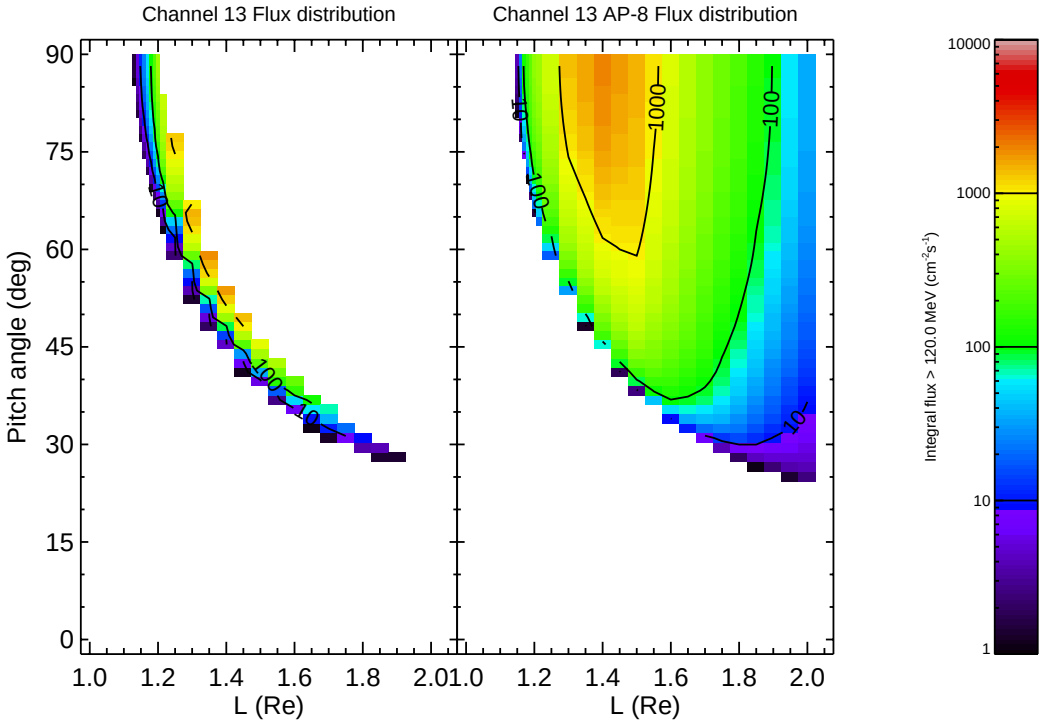

Figure 5.8. (L, α_0) Map of the PSB97 model and AP-8 MIN for channel 13

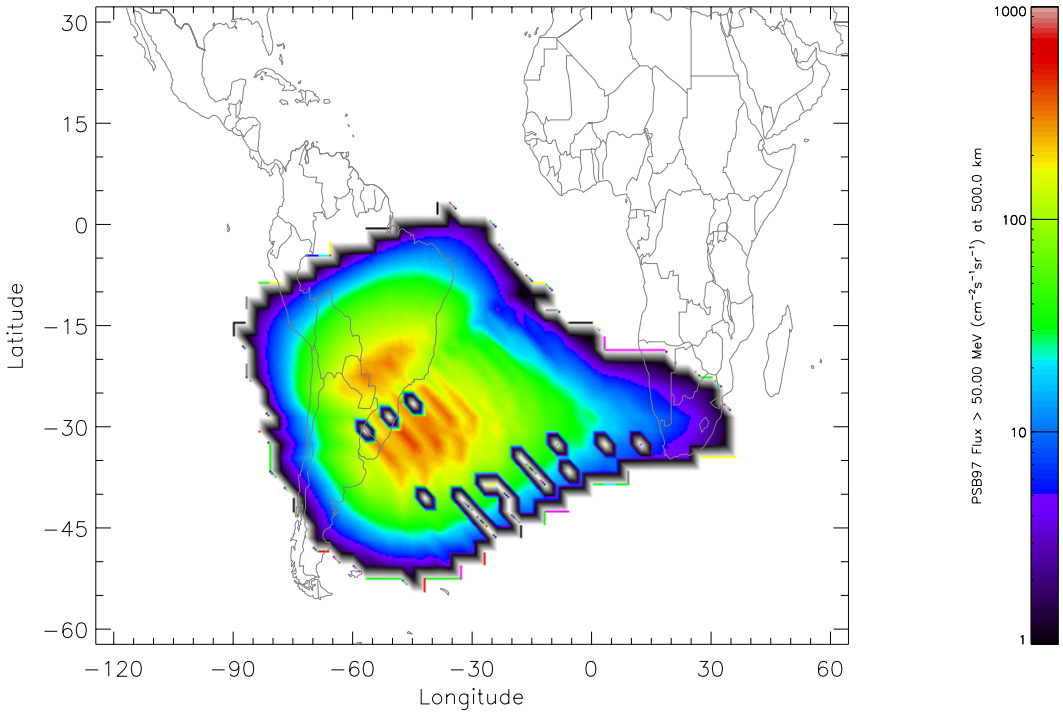

Figure 5.9. World map of the PSB97 >50 MeV proton flux at 500 km

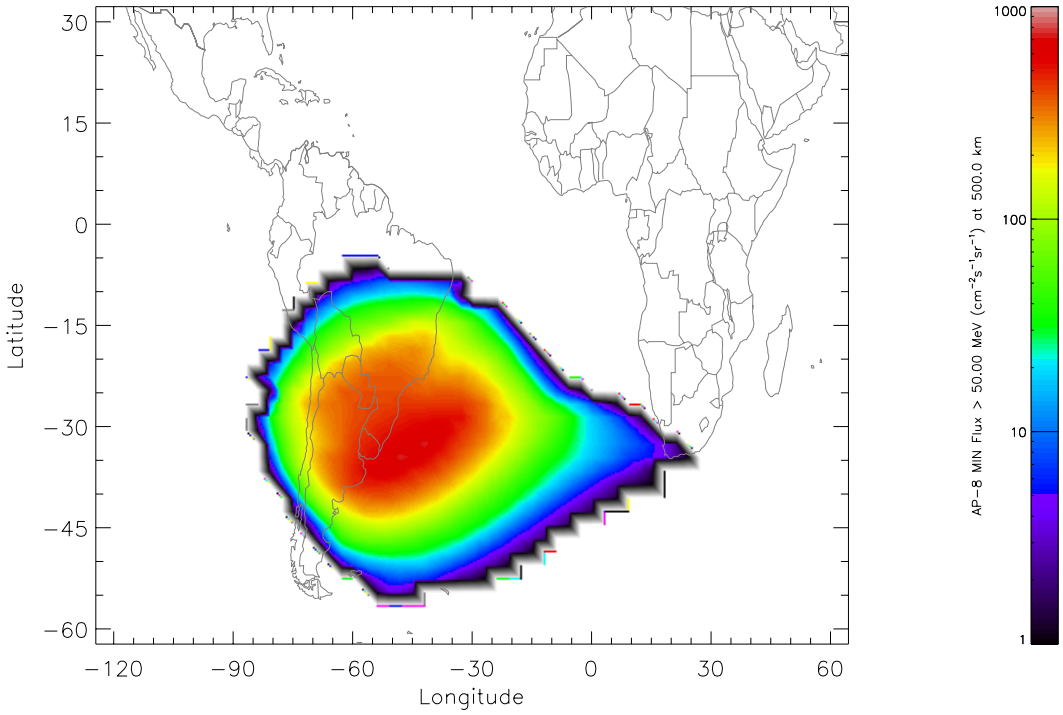

Figure 5.10. World map of the AP-8 MIN >50 MeV proton flux at 500 km

It can be seen that for the lowest L values the PSB97 fluxes are smaller than the corresponding AP-8 MIN fluxes by a factor of about two.

Another way of comparing the PSB97 model to AP-8 consists of drawing world maps of fluxes at fixed altitude. Figures 5.9 and 5.10 show the distributions of the PSB97 and AP-8 MIN proton flux >50 MeV at an altitude of 500 km, respectively. Again, the PSB97 flux is lower than the AP-8 MIN flux.